Naval Research Laboratory
Washington, DC 20375-5000

NRL Memorandum Report 6203

Calculated Radar Images of Ship Wakes From Simulated Wake Hydrodynamic Models

DENNIS B. TRIZNA

Radar Propagation and Scattering Staff
Radar Division

GEORGE KERAMIDAS

Laboratory for Computational Physics and Fluid Dynamics

March 24, 1989

SECURITY CLASSIFICATION OF THIS PAGE

AD-A207579

REPORT DOCUMENTATION PAGE

Form Approved OMB No. 0704-0188

1a. REPORT SECURITY CLASSIFICATION: UNCLASSIFIED	1b. RESTRICTIVE MARKINGS
2a. SECURITY CLASSIFICATION AUTHORITY	3. DISTRIBUTION / AVAILABILITY OF REPORT: Approved for public release; distribution unlimited.
2b. DECLASSIFICATION / DOWNGRADING SCHEDULE	
4. PERFORMING ORGANIZATION REPORT NUMBER(S): NRL Memorandum Report 6203	5. MONITORING ORGANIZATION REPORT NUMBER(S)
6a. NAME OF PERFORMING ORGANIZATION: Naval Research Laboratory; 6b. OFFICE SYMBOL (If applicable): Code 5303	7a. NAME OF MONITORING ORGANIZATION
6c. ADDRESS (City, State, and ZIP Code): Washington, DC 20375-5000	7b. ADDRESS (City, State, and ZIP Code)
8a. NAME OF FUNDING / SPONSORING ORGANIZATION: Office of Naval Research; 8b. OFFICE SYMBOL (If applicable): ONR	9. PROCUREMENT INSTRUMENT IDENTIFICATION NUMBER
8c. ADDRESS (City, State, and ZIP Code): Arlington, VA 22217	10. SOURCE OF FUNDING NUMBERS: PROGRAM ELEMENT NO. 61153N; PROJECT NO. RR021--05-43; TASK NO.; WORK UNIT ACCESSION NO. DN280-045

11. TITLE (Include Security Classification)
Calculated Radar Images of Ship Wakes from Simulated Wake Hydrodynamic Models

12. PERSONAL AUTHOR(S)
Trizna, D.B. and Keramidas, G.

13a. TYPE OF REPORT	13b. TIME COVERED	14. DATE OF REPORT (Year, Month, Day)	15. PAGE COUNT
Interim	FROM 1/85 TO 6/87	1989 March 24	26

16. SUPPLEMENTARY NOTATION

17. COSATI CODES			18. SUBJECT TERMS (Continue on reverse if necessary and identify by block number)
FIELD	GROUP	SUB-GROUP	Ship wakes; Radar image; SLAR image and sea scatter

19. ABSTRACT (Continue on reverse if necessary and identify by block number)

Calculations of radar scatter images from simulated ships wakes are presented for two ships, the Quapaw and a DDG class vessel. Three ship speeds were used for each, scaled so that the Froude numbers were the same for both vessels. Two radar scattering mechanisms were used: Bragg scatter and an empirical sea spike model. No Doppler effects are considered (important to SAR image formation) so that the model is one for a real-aperture radar. Both vertical and horizontal transmit polarizations were used, with like polarizations received, for a single depression angle of 45 deg. degrees. Two flight aspects were considered: parallel and perpendicular to the axis of the wake, with the radar beam perpendicular to the direction of flight. Simulated wake elevations and slopes are calculated using the slender ship method published recently by Keramidas (1987). The results show a relatively weak modulation from the Bragg scatter contribution, which would probably be masked by moderate sea conditions. The most significant result is the occurrence of the maximum image brightness from a narrow V-wake. This image feature is associated with a region of large slope, but moderate wave height, due to the interaction of the superposition of the Kelvin wakes from the bow, stern, and ship body contributions. Because of the aspect of the high slope region, the radar echo from this region is significant only

(Continues)

20. DISTRIBUTION / AVAILABILITY OF ABSTRACT	21. ABSTRACT SECURITY CLASSIFICATION
☒ UNCLASSIFIED/UNLIMITED ☐ SAME AS RPT ☐ DTIC USERS	UNCLASSIFIED
22a. NAME OF RESPONSIBLE INDIVIDUAL: Dennis B. Trizna	22b. TELEPHONE (Include Area Code): (202) 767-2003; 22c. OFFICE SYMBOL: Code 5303

DD Form 1473, JUN 86 — Previous editions are obsolete. — SECURITY CLASSIFICATION OF THIS PAGE

S/N 0102-LF-014-6603

PAGES _____

ARE

MISSING

IN

ORIGINAL

DOCUMENT

19. ABSTRACTS (Continued)

for radar beam illumination perpendicular to the wake axis. For perpendicular flight aspect, the radar image consists primarily of the Bragg return for both polarizations and yields only the Kelvin wake. Suggestions are made for improving both the radar scatter model and the hydrodynamic model. Keywords: Tugboats radar images; Guided missile ships; Side-looking airborne radar; Flight paths; → Sea clutter (edc)

CONTENTS

CALCULATED RADAR IMAGES OF SHIP WAKES FROM SIMULATED WAKE HYDRODYNAMIC MODELS

INTRODUCTION

While imaging of ship wakes with synthetic aperture radar has been done for more than twenty years, a satisfactory model describing the essential features of these images has never been presented. The most difficult observation to explain has been the very narrow wake angle observed in the radar images, with virtually little or no sign of the Kelvin wake, with its 38.9^0 wake angle. A second observation is the lack of a radar image for radar illumination aspects parallel to the wake core. In this work, we present calculations which produce these characteristics.

The simulation combines the results of radar scatter calculations and hydrodynamic calculations for ship wakes for two vessels, a wide-beam tug and a destroyer. The calculated images use relatively simple assumptions for the radar scatter model: a two-scale model using Bragg scatter, and an empirical sea spike model. The essential features of wake images produced here appear to be primarily due to new results in the details of the wake structure produced by a hydrodynamic calculation of the flow field around a ship, which yields a linear gravity-wave representation. The narrow wake features are a result of very steep waves predicted by the hydrodynamic model, which are assumed to break, producing a sea spike radar return at that pixel. The details of the hydrodynamic and radar calculations are given below, and radar simulations are presented in the form of color coded images representing normalized radar cross section. Suggestions for improvements in the model are made in the discussion.

HYDRODYNAMIC MODEL

The flow field around a body moving at a near free surface and at constant speed can be computed from the solution of Laplace's equation with linearized free surface boundary conditions. Solutions to this problem can be obtained by a variety of methods. The one that is most commonly used by researchers in ship hydrodynamics is based on a simplified version of the panel method, where the surface of the body is divided into a set of triangular or rectangular panels with linear source strength distribution. The source strengths are not computed as part of the solution, but they are specified as inputs to satisfy the potential flow equations, i.e. Laplace's equation and the free surface conditions. The values of the source strengths for each panel can be specified according to either the Thin Ship theory or to the Slender Ship theory. In the present study we elect to use the Slender ship approximation, according to which the source strength density of a surface panel is proportional to the product of the forward speed U of the ship and the longitudinal component of the unit normal vector to that panel. A detailed description of the Slender Ship theoretical analysis and formulation can be found in Noblesse (1983).

The implementation of the above theory into a usable computational tool consists of several steps, requiring numerical approximation of a number of integral quantities, and results in the computation of the total free surface spectral density due to all points along the ship's hull. This density function is then used to calculate the resultant Kelvin wave field by applying an inverse Fourier transform, resulting in the free surface elevation pattern and the x- and y-slopes of the pattern for each pixel. The result of contributions from the entire hull structure will produce interfering terms which can cause the wake profile to differ significantly from the classical results due to a point source. Details of these

Manuscript approved November 17, 1988.

calculations are given in Keramidas and Bauman (1987).

Examples of the elevation, x- and y-slopes are shown in Figs. 1a, 2a, and 3a for a tug, the Quapaw (wide hull example) at a speed of 16 kts, and for a destroyer (slender hull example), in the corresponding b-figures for a speed of 25 kts. The 19.5^0 classical wake lines from the stern and bow are shown as the wide sets of overlaid parallel lines, while wake lines of 9^0 and 4.5^0 from the bow are also shown for comparison. Pixel sizes used are roughly two meters on a side, but not exactly the same size because of the format of the hydrodynamic calculation. They are displayed on a square format however. The overlays are in the reference frame of the calculations and track the wake correctly.

RADAR SCATTERING MODEL

One of two models for radar scatter were used for each pixel, with the choice determined as follows. For each pixel, the surface was assumed to be a plane with the x- and y-slopes given by output from the hydrodynamic wake model. The x- and y-slopes are projections of the surface normal of the pixel onto the vertical co-ordinate planes. A breaking wave was introduced whenever the greater of the x- or y-slope was greater than 0.356, and a sea spike model was then used to calculate the radar echo amplitude. For cases not satisfying the wave breaking criterion, a Bragg scatter model was used. The capillary spectral density for the Bragg scatter was calculated using a wind speed dependent model given by Fung and Lee (1982). Extension to three dimensions of the models requires mixing horizontally and vertically polarized fields, similar to that considered by Valenzuela (1968), but using x and y-slopes as inputs. The relation between these slopes and Valenzuela's tilt angles are defined.

1. Bragg Scatter Model

The following expression was used to predict the radar Bragg scatter amplitude in a given pixel (Wright, 1968):

$$\sigma_{ij}{}^0 = 4\pi k^4 \cos^4\Phi_r \, |g_{ij}|^2 \, W(K_{Bragg}, 0) \qquad (1)$$

where

k is the radar wave number, $= 2\pi/\lambda$, with λ being the radar wavelength;

Φ_r is the local incidence angle at the scattering patch;

g_{ij} are first order scattering coefficients for horizontal and vertical polarizations;

$W(K_{Bragg}, 0)$ is the two dimensional ocean wave spectra density in cartesian co-ordinates; and

$K_{Bragg} = 2\,k \sin\Phi_r$ is the water wavelength responsible for the resonant scatter.

The scattering problem for a three dimensional surface requires attention to mixing of polarizations, various combinations of i and j, in order to calculate the scattered radiation. To simplify the calculations we shall consider only the cases of illumination by radar illumination parallel and perpendicular to the axis of symmetry of the ship wake. For these cases, the slopes calculated from the hydrodynamic model can be simply implemented. For each pixel the normal to the planar surface can be projected onto the xz and yz-planes. For purposes of the radar scattering code these two

projected vectors then provide inputs to the calculation of the tilt modulation and polarization mixing, allowing the calculated x- and y-slopes to be incorporated into the scattering model in a straightforward manner. Valenzuela (1968) has calculated the scattering coefficients for tilt, but the reference frame used is not appropriate to our needs.

The hydrodynamic calculation produces the local slope angles relative to a reference frame in which the x and y-axes are perpendicular and parallel to the direction of travel of the ship, which we refer to as the direction of the axis or core of the wake. The geometry for a local pixel component of the wake is shown in Fig. 4a, with the x-axis pointing toward the ship in the images of Figs. 1-3, and the y-axis to the right. Each of the projections of the surface normal are shown in Figs. 4b and 4c, with corresponding planes drawn for illustration. For an arbitrary plane surface, the normal vector is given in polar coordinates by:

$$\mathbf{n} = (\cos\theta \sin\phi,\ \sin\theta \cos\phi,\ \cos\phi) \qquad (2)$$

The normalized projections onto the xz and yz planes are:

$$n_{xz} = (\cos\theta \sin\phi,\ 0,\ \cos\phi)/(\cos^2\phi + \sin^2\theta \cos^2\phi) \qquad (2b)$$

$$n_{yz} = (0,\ \sin\theta \sin\phi,\ \cos\phi)/(\cos^2\phi + \sin^2\theta \cos^2\phi) \qquad (2a)$$

The local slope angles for each of these component surfaces are then related to the slopes provided by the hydrodynamic calculations as follows :

$$dz/dx = \tan\psi = \cos\phi \ /\ (\ \cos\theta \sin\phi\ ) \qquad (3a)$$

$$dz/dy = \tan\delta = \cos\phi \ /\ (\ \sin\theta \sin\phi\ ) \qquad (3b)$$

The corresponding angles are related to the polarization mixing angle, δ', and the tilt modulation angle, ψ', of Valenzuela by $\cos\delta' = \cos\delta \cos\psi$, and $\psi' = \psi$ which will be derived in another work.

2. Shadowing by Steep Wave Crests

Consider next shadowing of the incident energy by the crest of a steep wave for a given radar illumination geometry. For the case of the radar flying along the axis of the wake (in the positive x direction), the radar wave vector is pointed perpendicular to the wake axis. For this case, the normal vector of the y-slope contribution lies in the xz plane, as shown in Fig. 4b. For cases where the angle between this normal vector and radar wave vector are equal to or greater than 90^0, shadowing occurs. In this treatment, we assign a minimum RCS value to this shadowed pixel, but do not consider whether or not the pixel following in radar range is shadowed, which a more exact model must do. For the case where the ocean wave slope angle is less than 70^0, relative to the z-axis, which corresponds to wave slopes angle of 20^0 and 0.34 maximum slope, the wave is assumed to be

breaking and a sea spike normalized radar cross section (NRCS) value is assigned, which is described next.

3. Sea Spike Model

In Fig. 3, it is apparent that the hydrodynamic model predicts wave slopes that are greater than that required for breaking, roughly 0.34 for a 20^0 slope. This is a result of the linearity of the hydrodynamic calculation. To account for the occurrence of wave breaking in the radar imaging, we assume that for x- or y-slope greater than 0.34, Bragg scatter no longer holds. Instead, we assume that the gravity wave has broken, and that it produces radar scatter amplitudes of the order of those observed for sea spike radar returns. (See, for example, Trizna (1987); Hansen and Cavaleri (1982); Lewis and Olin (1980)). Because no widely accepted model exists which predicts the radar scatter amplitudes from a breaking wave for so high an incidence angle, we have simply set the NRCS to 0 dB times an azimuthally dependent factor discussed next. Such an NRCS magnitude serves only to map the occurrence of the sea spikes, and to provide directional dependence for comparison with general aspect angle characteristics of the radar imagery.

Assumptions about the scale size of the scatterer are necessary to explain the lack of occurrence of a narrow wake radar image for the radar flying perpendicular to the wake core. To satisfy this observation, the sea spike model requires an azimuthal variation of the scatter that is neither omni-directional nor uni-directional. An omni-directional sea spike scatterer would yield narrow wake images of identical intensity for all azimuthal observation angles. A uni-directional scatter model would allow backscatter only for azimuthal incidence in the vertical plane containing the pixel normal. Such a scattering surface would not provide a sufficient number of pixels to image a narrow wake in any direction because of the very small number of pixels with slopes preferentially aligned in that specific direction. The steepest pixels calculated in the hydrodynamic model have normals at angles δ=90^0 and ψ from 30^0 to 45^0 for regions in the narrow wake, with small x-slope and large y-slope, (Figs. 2 and 3). Thus, a scattering model which allows for a narrow beamwidth of scatter centered on the pixel normal will produce a narrow wake image as described earlier.

One can produce such NRCS azimuthal behavior using a scattering feature which has a coherence length several radar wavelengths across, in a fashion similar to that for defining an antenna beamwidth. The elevation angular dependence will be a function of the variation of the surface features in the plane containing the pixel surface normal, which we do not consider here. A beam shape is achieved for the simplest case, a crest of coherence length 'a', which is proportional to the coherence length, given by antenna theory (See, for example, Skolnik, 1982):

$$G(\theta) = \mathrm{sinc}(1/2\ ka\ \sin\theta) \qquad (4)$$

where sinc x = (sin x)/x. The beamwidth of this pattern at half power points is 51 λ/a degrees. In these calculations, we have chosen a crest length of the order of five wavelengths, yielding roughly a 10^0 beamwidth at X-band, an arbitrary choice for example only. Comparison with real images could allow this width as an empirical input parameter, or in-situ wave crest measurements could be used as an input instead.

RESULTS

With these relatively crude assumptions in the radar scatter model, the essential features of radar images of wakes can be produced using the hydrodynamic simulations. In the following, the RCS value is calculated for each pixel provided by the hydrodynamic calculations, each pixel represented by a flat plane with a specific elevation and two orthogonal surface slopes. The hydrodynamic results were obtained by assuming a perfectly flat background sea at long wavelengths, with small scale surface roughness due to a wind speed of 7 m/s, or roughly 14 kts. This provides a small scale surface roughness for the composite model, but no long waves to compete with the wake gravity wave structure.

i. Quapaw - Radar Illumination Beam Parallel to Ship Bearing

Fig. 5a and 5b show simulated radar images for horizontal and vertical polarization for the Quapaw wake simulations of Figs 1b, 2b, and 3b. The flight direction is perpendicular to the ship heading, with the radar beam pointing parallel to the wake core from a point forward of the ship. The image for vertical polarization of Fig. 5a appears to closely resemble the X-slope pattern of Fig. 2b, but with the higher cross section (pink colors in Fig. 5a) associated with the negative slopes (blue colors in Fig. 2b). In this pink region in Fig. 5a, illumination from a point forward of the ship results in the smaller depression angles (closer to the normal) for negative surface slopes, and yields the largest composite scatter echo according to Eq. 1. The transverse wave components image most strongly for this illumination aspect.

The terms producing the modulation in Eq. 1 are the cosine-fourth term, the g_{ij} term, and the resonant spectral density, W, all dependent on the incidence angle. These all contribute to the tilt modulation effect. We do not treat the modulation of W by orbital motions, accountable by an empirical modulation transfer function approach. Note that the image modulation along the 19.5° wake lines is of the order of two dB, which would be of the order of the modulation due to a real ocean surface and would probably be masked by the surface wave image. The image modulations for horizontal polarization in Fig. 5a are weaker than 6b, and are due to the weaker g_{hh} variation in Eq. 1.

The region between the 4.5° and 9° lines drawn show several pixels with yellow and black colors, indicating RCS values of the order of ten dB and higher above the background. This is due to the very high X-slope values (black and yellow pixels) appearing in Fig. 2b, causing either severe tilt modulation, or a sea spike return (black pixels) in the RCS image. Figs. 6a and 67b show the same RCS images of 5a and 5b, but with 3-db steps to suppress the weaker modulations relative to the stronger pixels for viewing. The features between 4.5° and 9° are seen to stand out now. It is apparent that a "narrow wake" image results for both polarizations.

ii. Quapaw - Radar Illumination Perpendicular to Ship Bearing

Figs. 7a and 7b show horizontally and vertically polarized results for the Quapaw at 16-kt speed, but now for the radar beam perpendicular to the ship bearing, radar flying along the ship's course. Both are seen to closely resemble the Y-slope pattern of Fig. 3b now, again due to the tilt modulation by the Y slopes, and with even more abundant sea spike contributions. This is due to the higher Y-slopes which occur when compared

with X-slopes, as seen by comparing Figs 1b and 1c. The occurrence of sea spikes is displayed more clearly again in the 3-dB step images of the same data, shown in Figs. 8a and 8b.

Figs. 9a and 9b show results similar to 8a and 8b, but for 13-kt ship speed. Similarly, Figs. 10a and 10b are for a 10-kt ship speed and also for perpendicular illumination for the Quapaw.

iii. DESTROYER - Radar Illumination Parallel to Ship Bearing

Figs. 10a and 10b show RCS results for the highest destroyer speed, 25 kts, and radar beam parallel to the ship bearing and wake core, the analogues of Figs. 5a and 5b. The transverse waves image exceptionally well. The narrow V-wake is not as strong as for the Quapaw, a result of the weaker Y-slopes generated by this much narrower hull.

iv. DESTROYER - Radar Illumination Perpendicular to Ship Bearing

Figs. 12a and 12b show the 25 knot destroyer case for the radar beam perpendicular to the wake core. The sea spikes are seen to be much larger again for this illumination geometry than for the previous one, similar to the behavior for the Quapaw.

DISCUSSION

While these results produce reasonably good images with a minimum of assumptions, there is room for improvement in a more quantitative model for the two-scale model and the narrow wake sea spikes associated with the high slope regions. Scattering from the non-breaking features of the hydrodynamic model can be explained by Bragg scatter, except for the phase of the NRCS magnitude relative to the elevation magnitude. The modulation transfer function (MTF) formalism accounts for a spatial shift in the pattern of the radar image relative to elevation image (See, for example, Wright 1966). This formalism is empirical, as the current MTF model based on orbital wave modulation does not explain measurements satisfactorily. Because the MTF measurements in the literature are not fully consistent with one another, implementation of this improvement to our model is not warranted at this time (See, for example, Trizna and Wu, 1988).

A second area which requires further investigation is the calculation of wave slopes using a higher spatial resolution. In these results, the slopes change dramatically from one pixel to the next in the region of the narrow wake. This can be remedied by using higher pixel resolution in these regions. Also, wave breaking must also be treated using a more realistic model.

Finally, given an appropriate non-linear model for wave breaking in these regions, the calculation of the radar scatter from these features remains a problem, but one with great potential for information content. As the specific profile of the wave breaking and its development may not be tractable in the near future, radar measurements of these features may be the best solution in the near term. Nevertheless, some progress can be made using models and measurements for breaking waves currently available. For example, one can assume that the breaking mechanism occurs along the wave crest, producing a feature similar to that discussed by Wetzel (1987) in his one dimensional model. In this model for sea spikes, he postulates a breaking plume feature as a half cylinder of water rolling down the face of

the steep wave after breaking, the intersection of the half cylinder being perpendicular to the local wave slope, as shown in Fig. 13a. Trizna (1987) suggests that a mean local angle of intersection of the cylinder relative to the horizontal of two degrees, as shown in Fig. 13b, explains the sudden rise in sea spike cross section that he observed for grazing angles steeper than 2^0 (relative to the horizontal) in open ocean radar measurements of sea spikes. These detailed differences are probably not important at the higher angles of observation expected for a spaceborne SAR. However, such a detail may be important in finding an optimum angle of illumination for enhanced narrow wake detection for a given ship type and its expected narrow wake.

If one could detect the Kelvin wake using the Bragg scatter mechanism, the periodicity of the pattern would allow one to determine the ship's speed unambiguously, regardless of flight aspect of the radar to the wake core. In fact, the spatial pattern along with the NRCS magnitudes would in principle allow identification of the vessel, using a library of calculated wake patterns and radar images. However, the application of such a technique would require the calculation of the interaction of a wind wave spectrum with the wake pattern, which again might best be handled empirically with radar measurements under finite number of conditions, used as boundary conditions for a wider range of wake and image calculations. In any case, the results presented here appear to provide the first success at predicting radar NRCS patterns using simulations exclusively.

REFERENCES

1. Noblesse, F., 'A Slender Ship Theory of Wave Resistance', Journal of Ship Research, Vol. 27, No. 1, March 1983, pp. 13-33.

2. Keramidas, G. A. and Bauman, W. D., 'FFSW : A Computer Program for Far Field Ship Wave Calculations', NRL Memorandum Report 6007, Nov., 1987.

3. Fung, A.K. & K.K. Lee, 'A semi-empirical sea spectrum model for scattering coefficient estimation', IEEE J. Oceanic Eng., OE-7, pp. 166-176, 1982.

4. Wright, J. W., 'A new model for se clutter', IEEE Trans. Antennas Propagation, Vol AP-16, pp. 217-223, 1968.

5. Valenzuela, G.R., 'Scattering of electromagnetic waves from a tilted surface', Radio Science, Vol. 3, pp. 1057-1066, 1968.

6. Trizna, D. B., 'Measurement and interpretation of North Atlantic Ocean marine radar sea scatter', NRL Report 9099, 1988.

7. Hansen. J. P. and V.F. Cavaleri, 'High resolution radar sea scatter, experimental observations and discriminants', NRL Report 8857, March, 1982.

8. Lewis, B. L. and I. D. Olin, 'Experimental study and theoretical model of high resolution radar backscatter from the sea', Radio Science, Vol 15, pp. 815-828, 1980.

9. Skolnik, M. I., Introduction to Radar Systems, McGraw-Hill, New York,

1982.

10. Wetzel, L., 'Models for Electromagnetic Scattering from the Sea at Extremely Low Grazing Angles', NRL Memorandum Report 6089, December 1987.

11. Wetzel, L., 'On Microwave Scattering by Breaking Waves', in Wave Dynamics and Radio Probing of the Ocean Surface", Phillips & Hasselmann, ed. Plenum Press, N.Y., 1987.

12. Trizna, D.B. and Jin Wu, 'The modulation transfer function for Radar sea scatter - A two source model', (Submitted to Journal of Geophysical Research).

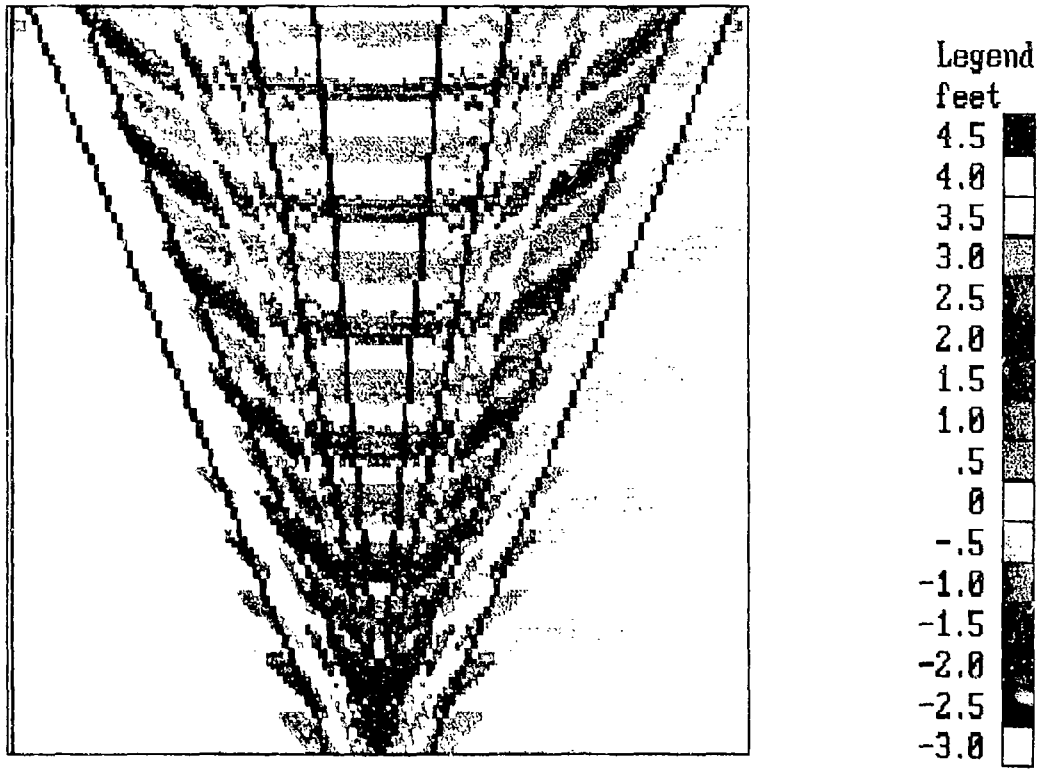

Fig. - 1a The elevation profile is shown of the wake generated by a destroyer moving at a 25 knot speed.

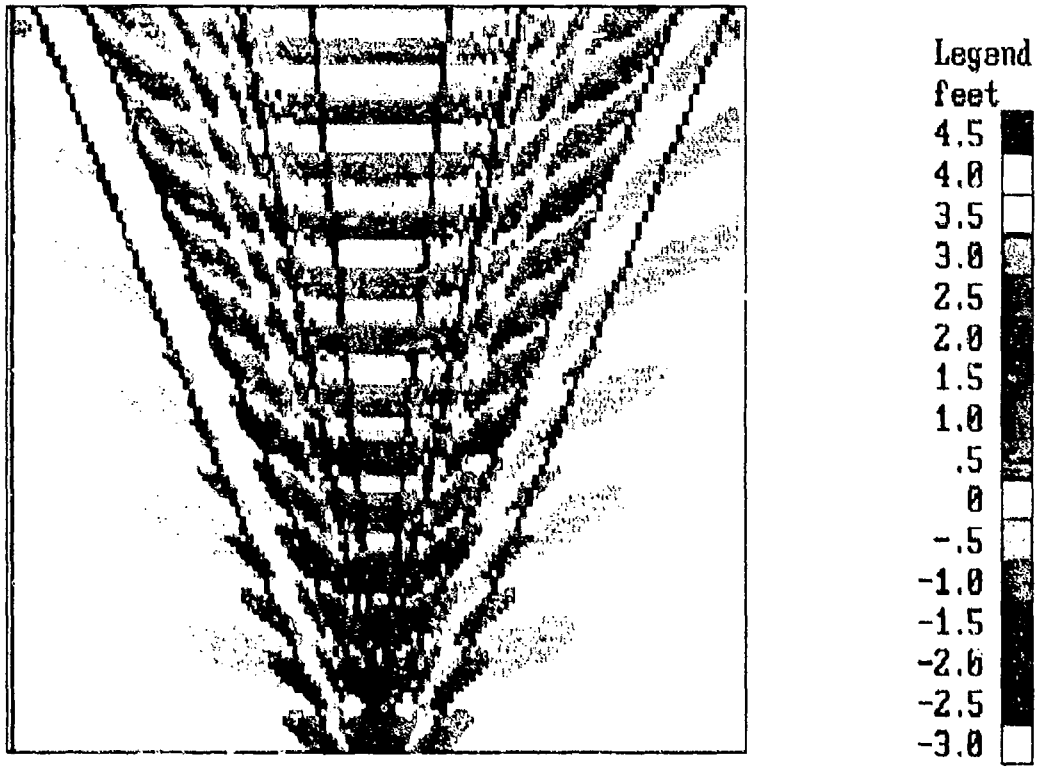

Fig. - 1b The elevation profile is shown of the wake generated by the Quapaw moving at a 16 knot speed.

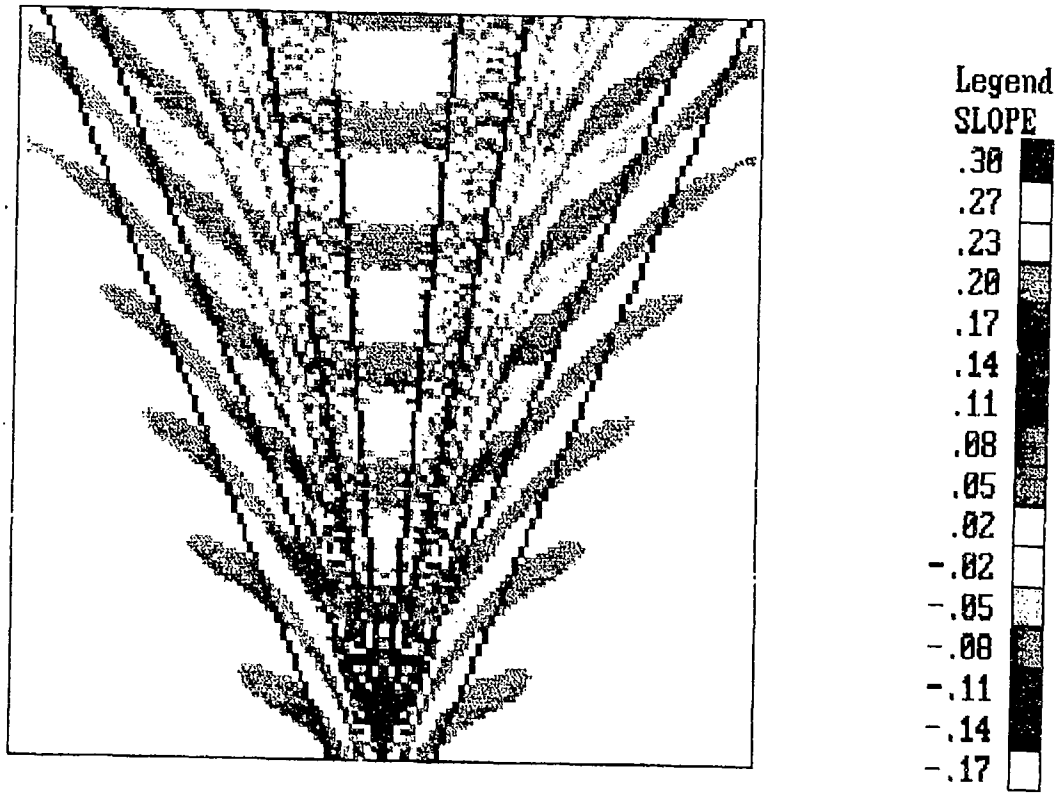

Fig. - 2a The pattern of slopes along the X-axis is shown for the conditions of Fig. 1a. The X-axis is parallel to the core of the wake, and thus is the axis of symmetry.

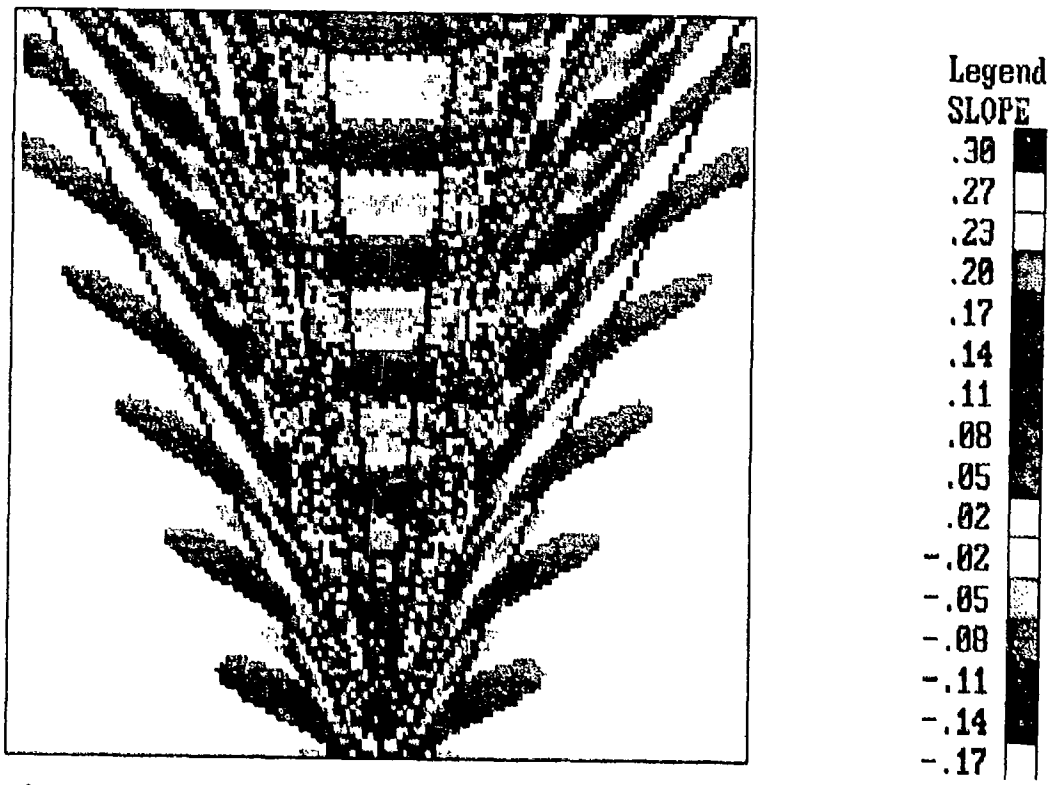

Fig. - 2b The pattern of slopes along the X-axis (X-axis parallel to the core of the wake) is shown for the conditions of Fig. 1b.

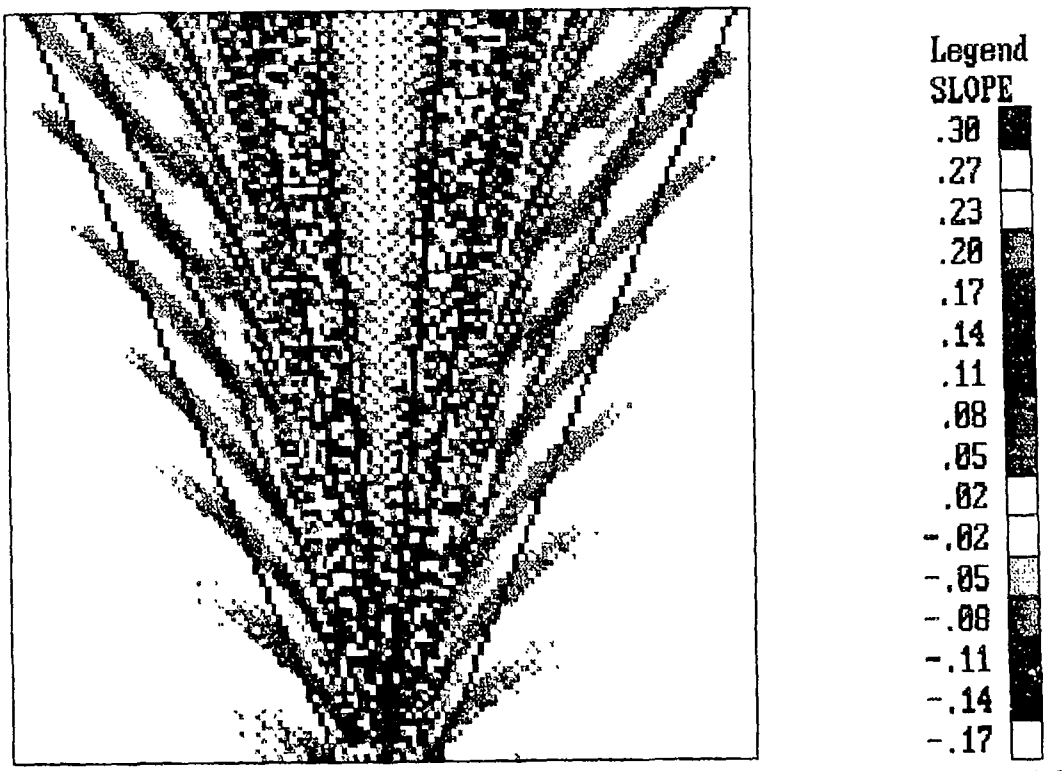

Fig. - 3a The pattern of slopes along the Y-axis (Y-axis perpendicular to the core of the wake) is shown for the conditions of Fig. 1a. Note the narrow V-pattern of high slopes inside the Kelvin wake.

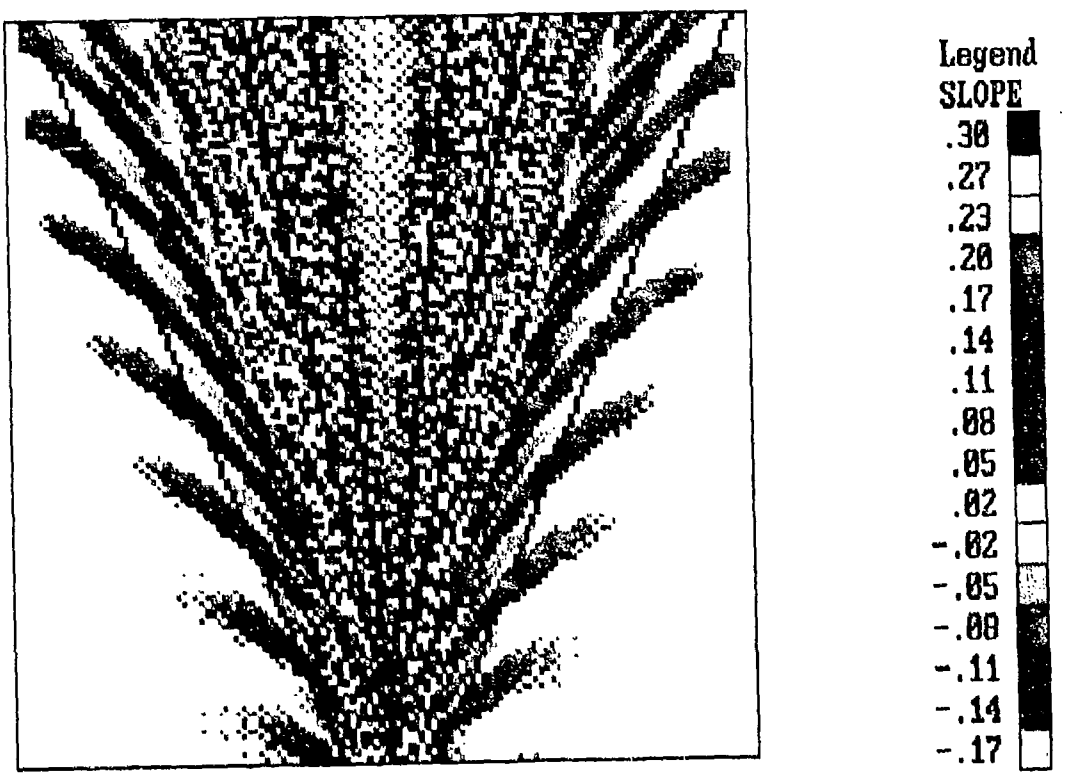

Fig. - 3b The pattern of slopes along the Y-axis (Y-axis perpendicular to the core of the wake) is shown for the conditions of Fig. 1b. The narrow V-pattern of high slopes inside the Kelvin wake is much more intense than that of the destroyer for the same Froude number.

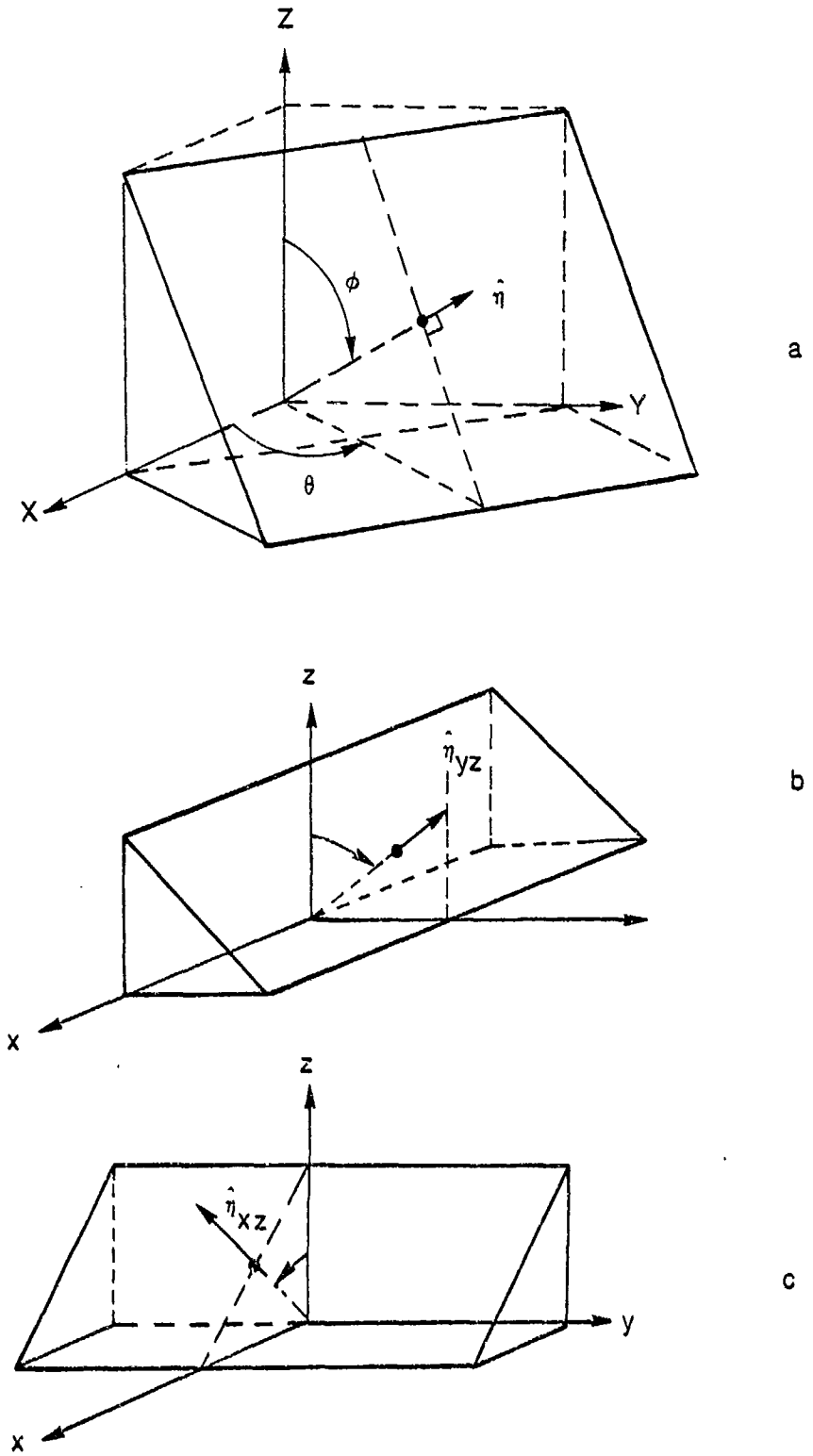

Fig. - 4 The geometry of a pixel and its normal vector in 4a, which is shown projected into the xz- and yz-planes in 4b and 4c. Planes in 4b and 4c are for illustration purposes only.

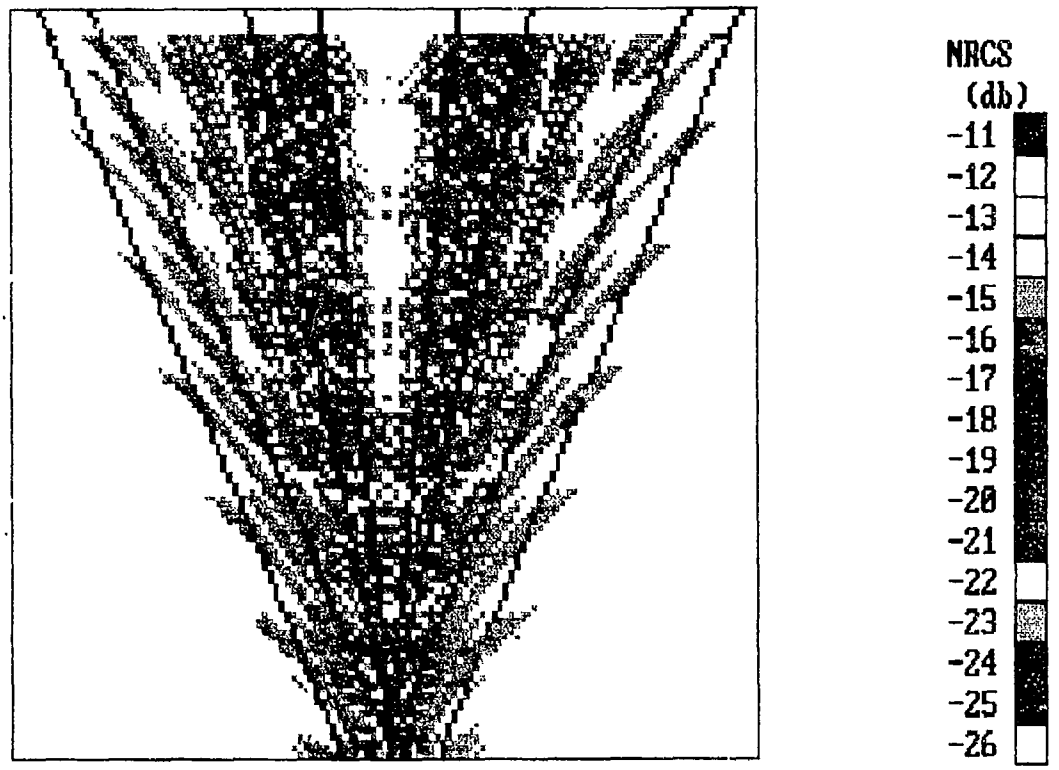

Fig. - 5a The NRCS image for horizontally polarized transmitted radiation, using the Quapaw wake presented in Figs. 1b-3b for a 16-knot speed, with radar illumination parallel to the axis of the wake.

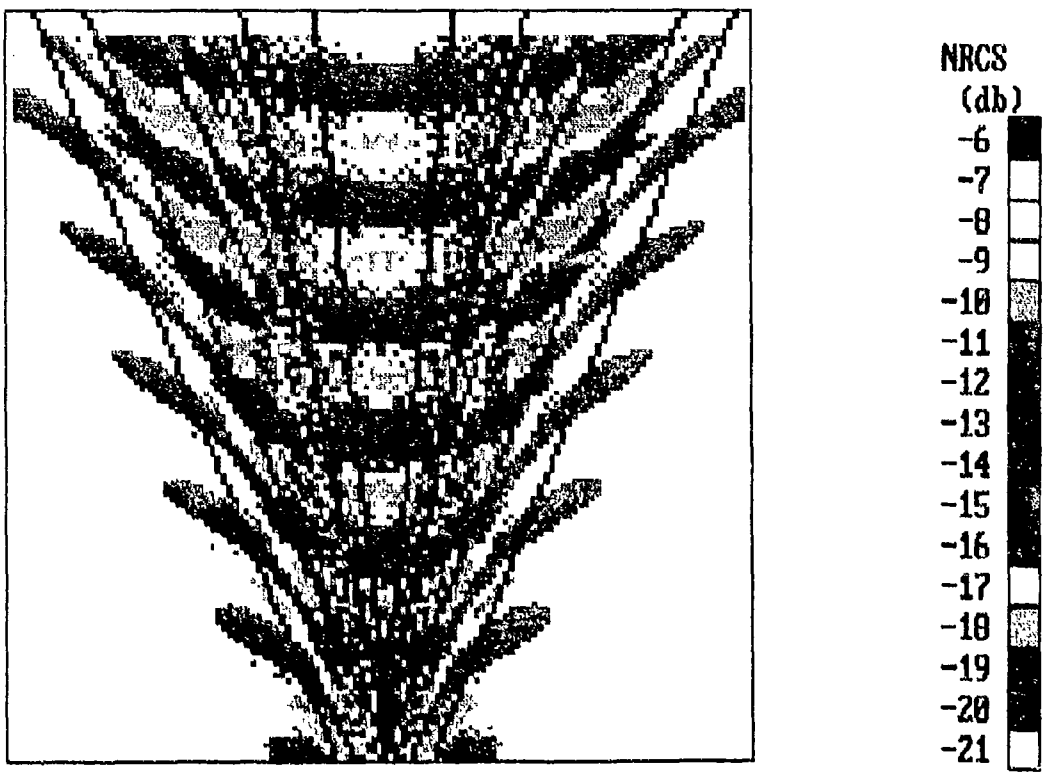

Fig. - 5b The same result as for Fig. 5a, but for vertically polarized incident radiation shown.

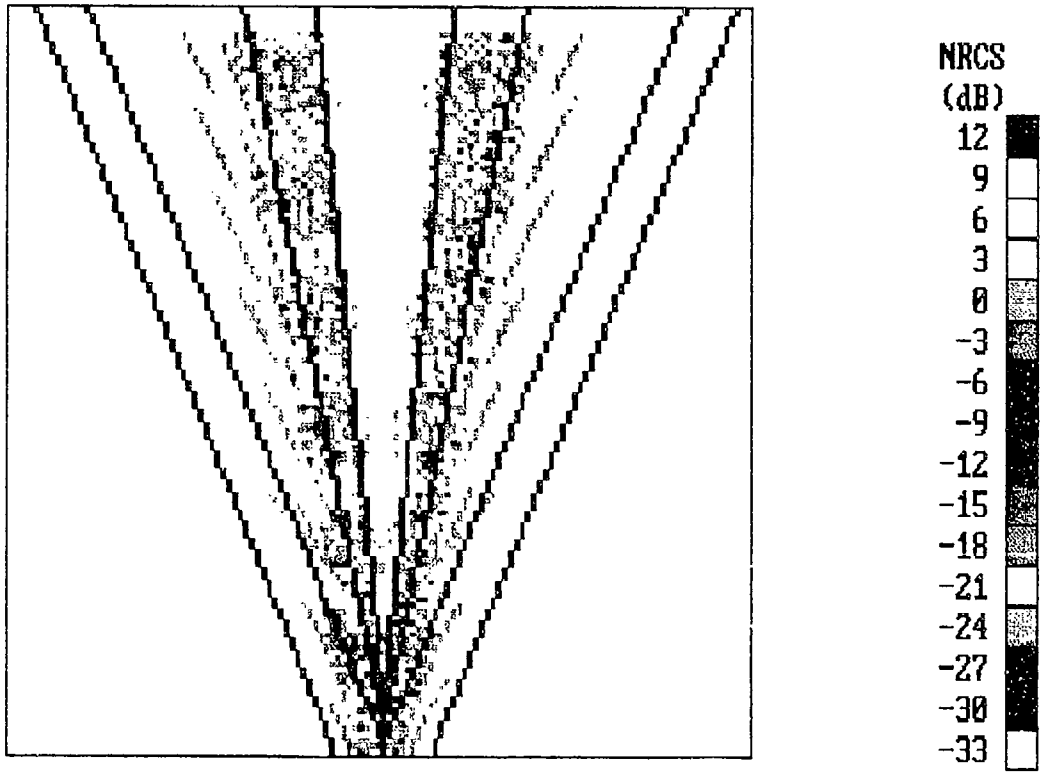

Fig. - 6a The same result as for Fig. 5a, but for 3-db steps instead to enhance the contrast between the narrow wake and the transverse wake.

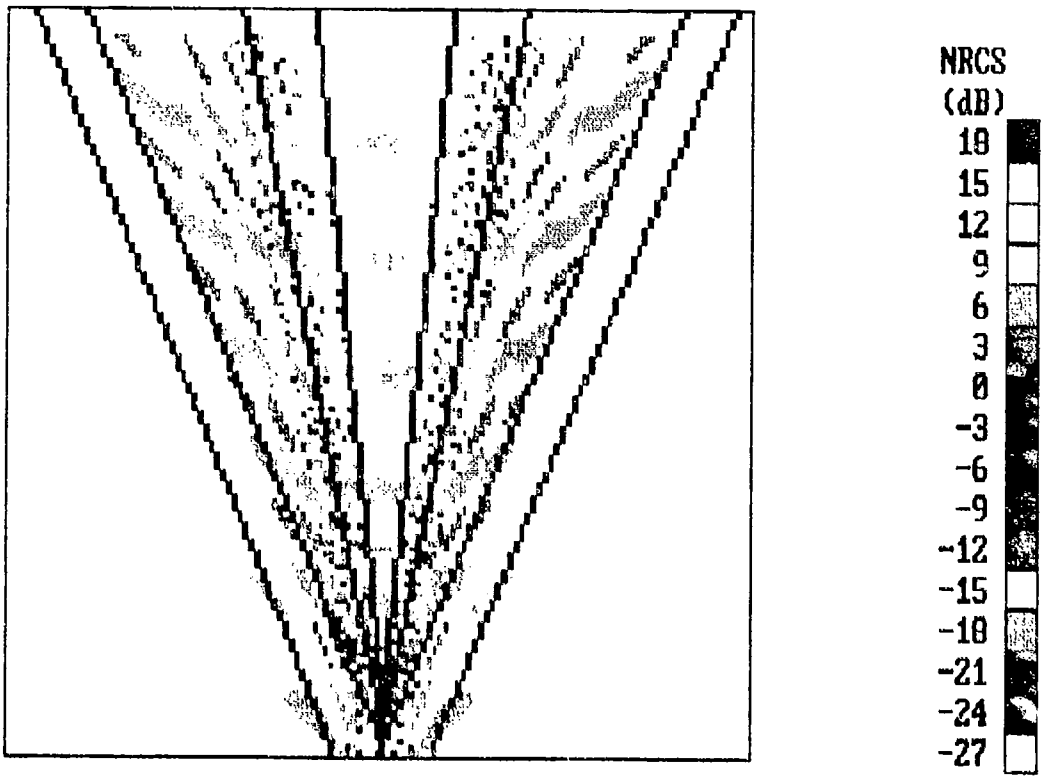

Fig. - 6b The same result as for Figure 6a, but for vertically polarized incident radiation.

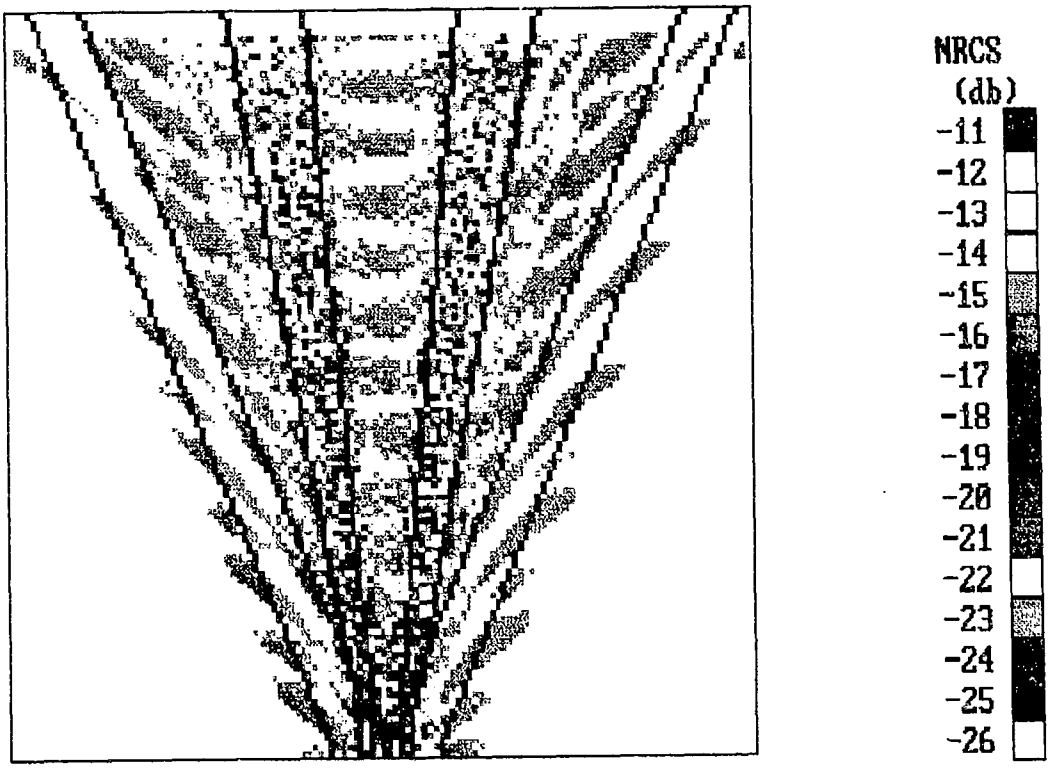

Fig. - 7a The same result as for Fig. 5a, but for radar illumination perpendicular to the ship wake core, showing an even strongler narrow V-wake region.

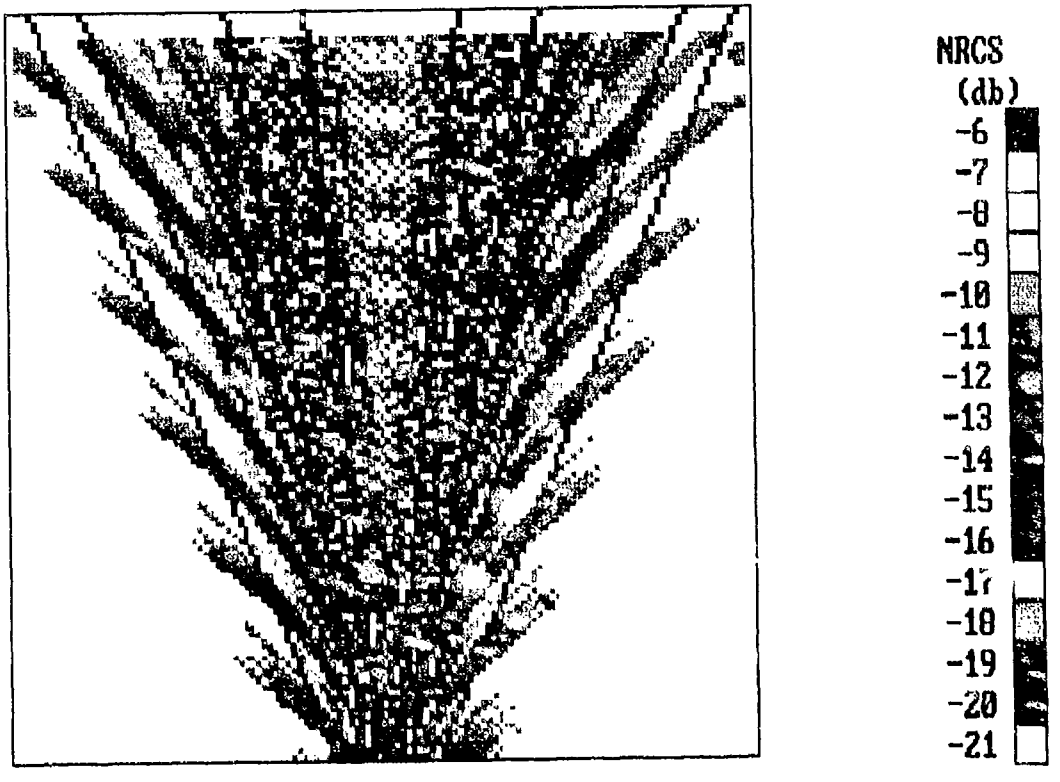

Fig. - 7b The same result as for Fig. 7a, but for vertical polarization.

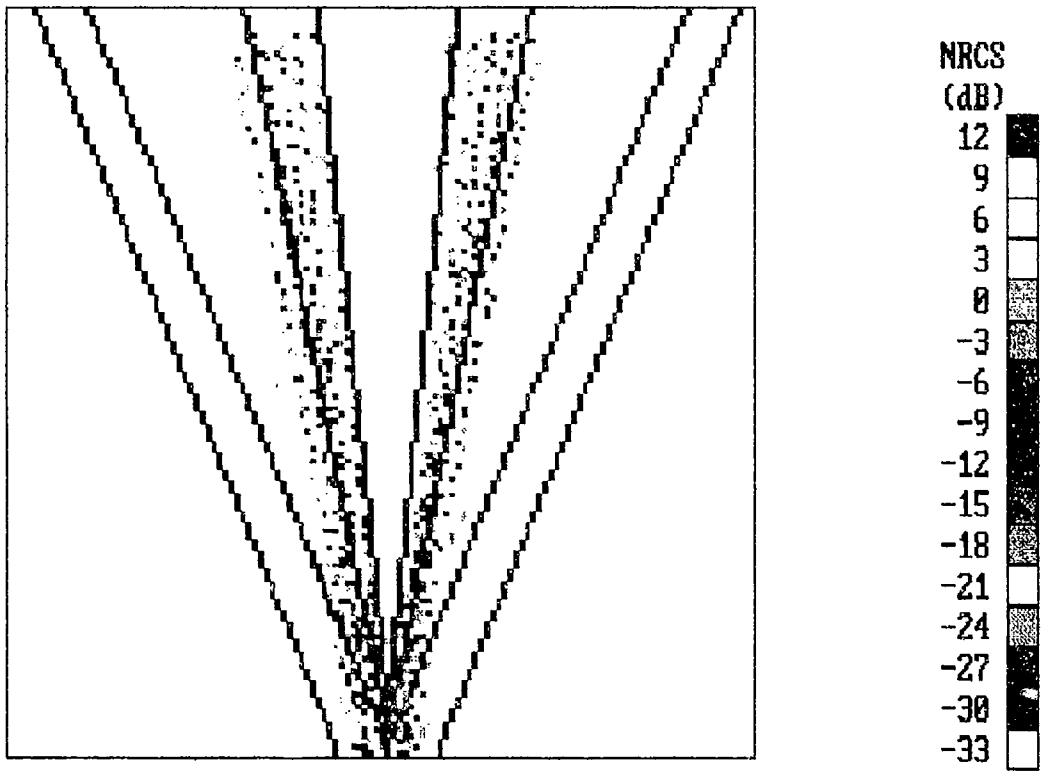

Fig. - 8a The same result as for Fig. 7a, but for a 3-dB step in color contour.

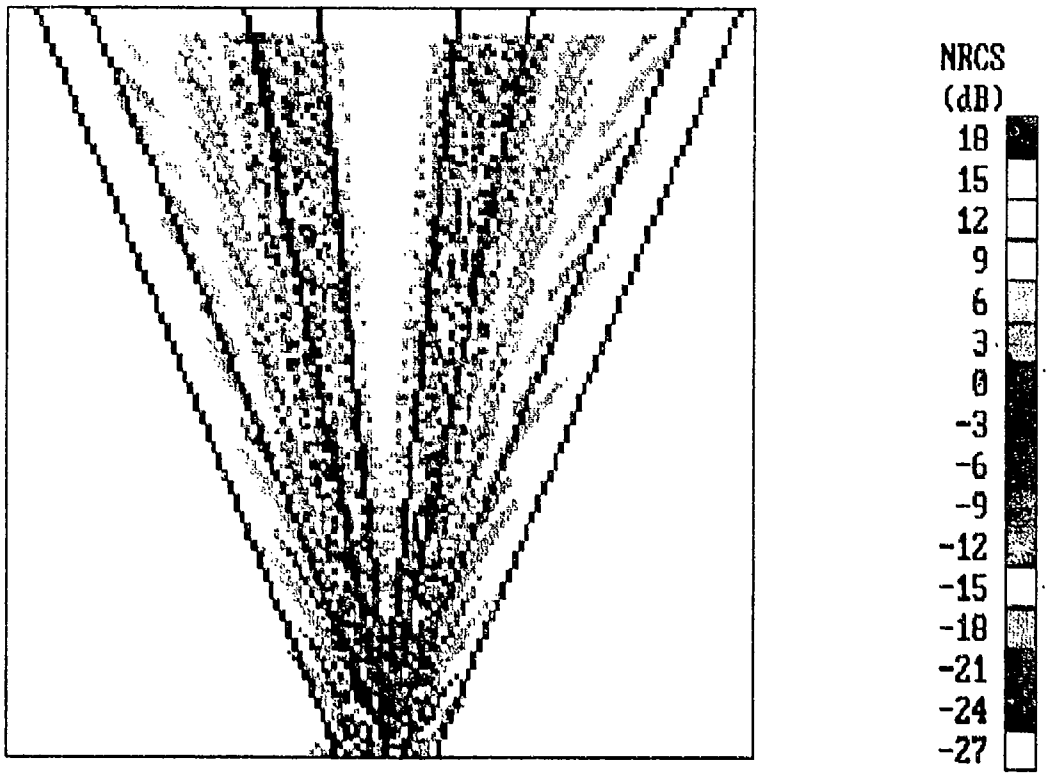

Fig. - 8b The same result as for Fig. 8a, but for vertically polarized incident radiation.

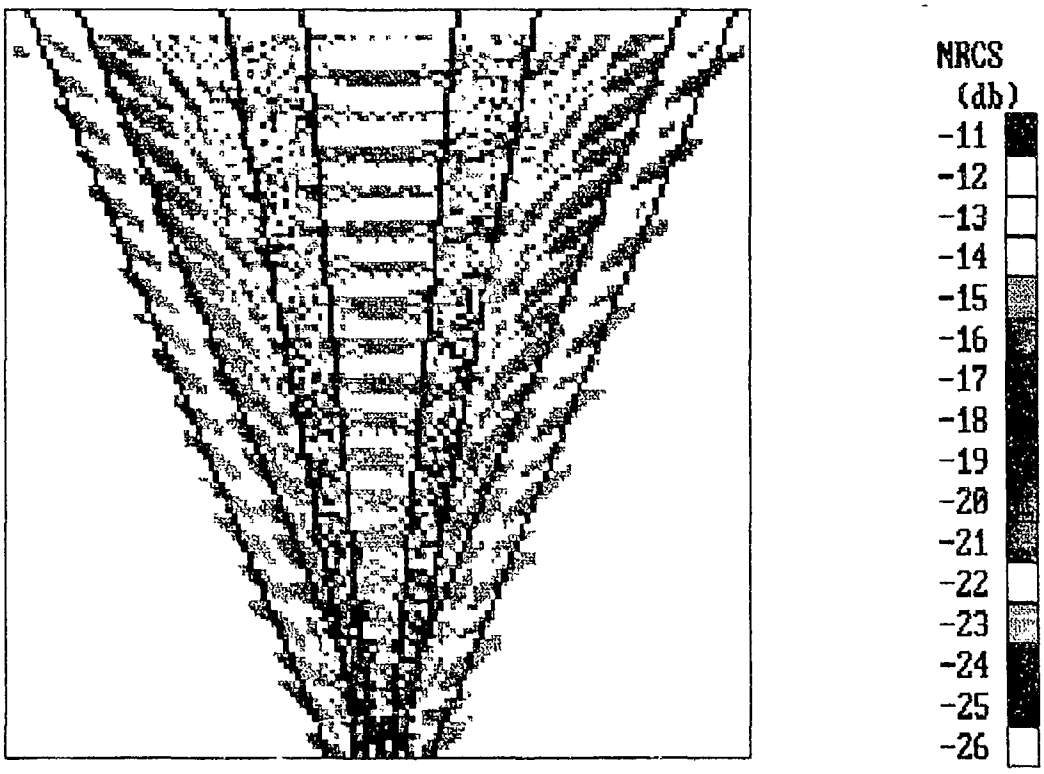

Fig. - 9a A result for the Quapaw at 13-knot wind speed, horizontal polarization, and radar beam perpendicular to the wake axis.

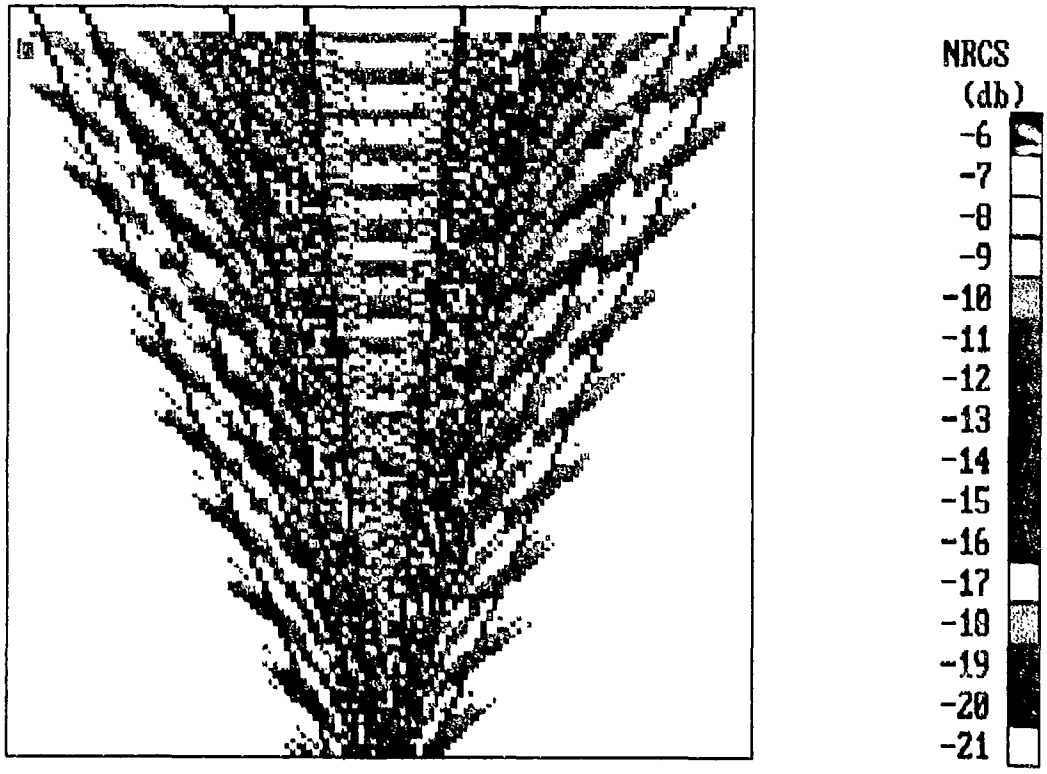

Fig. - 9b A result similar to 9a, but for vertical polarization.

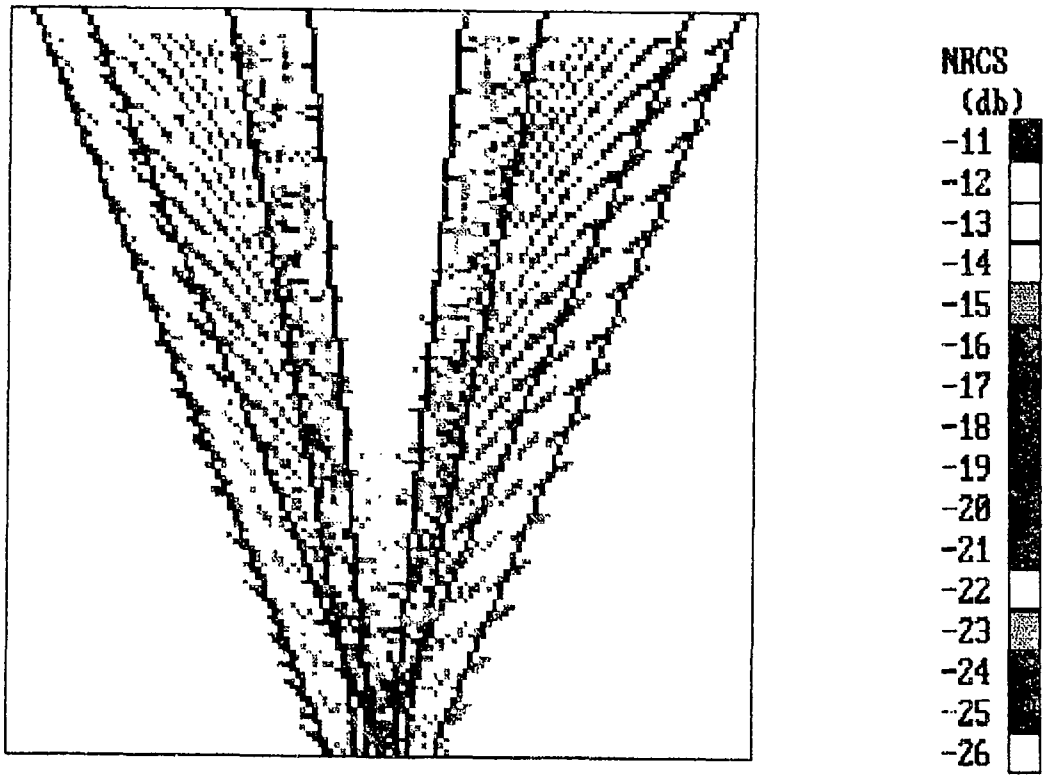

Fig. - 10a A result for the Quapaw at 10-knot wind speed, horizontal polarization, and radar beam perpendicular to the wake axis.

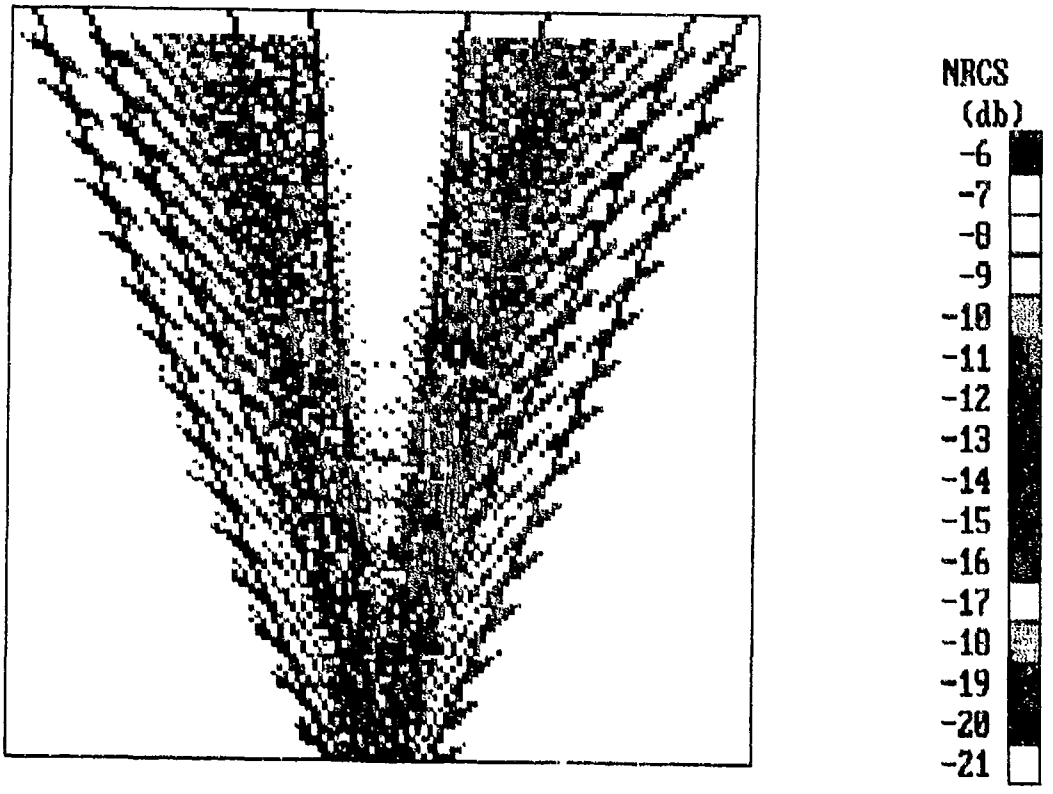

Fig. - 10b A result similar to 10a, but for vertical polarization.

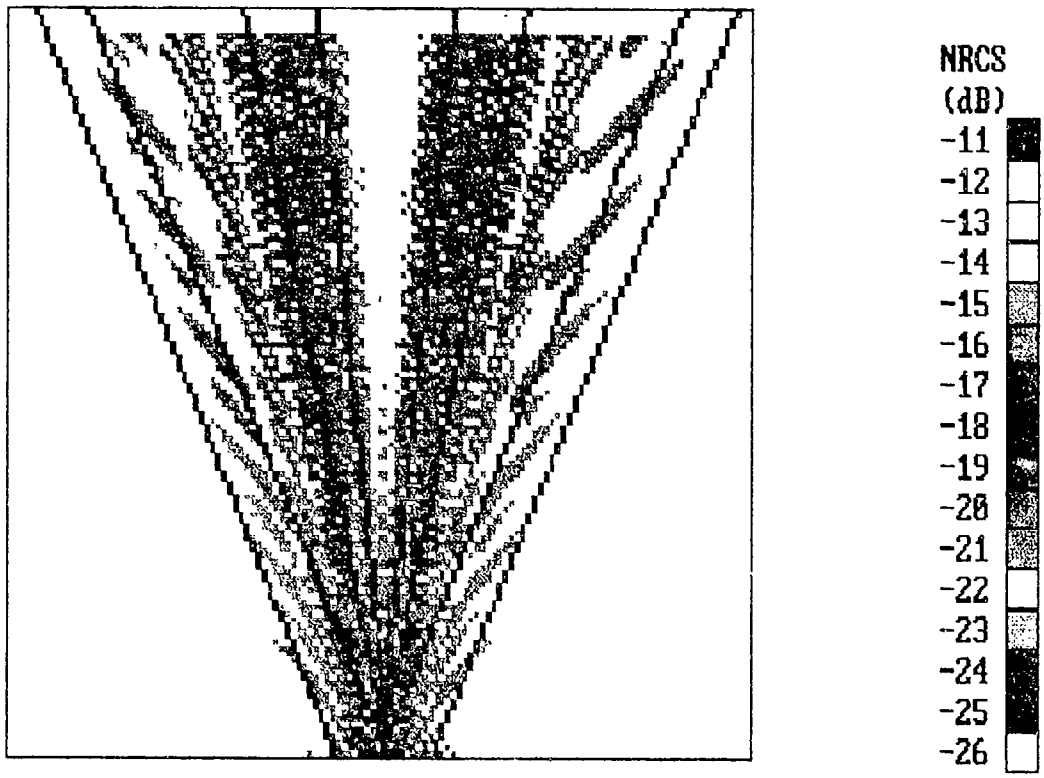

Fig. - 11a The calculated NRCS image for horizontally polarized transmitted radiation, using the wake presented in Figs. 1a-3a, the destroyer at a 25-knot speed, using radar illumination perpendicular to the axis of the wake.

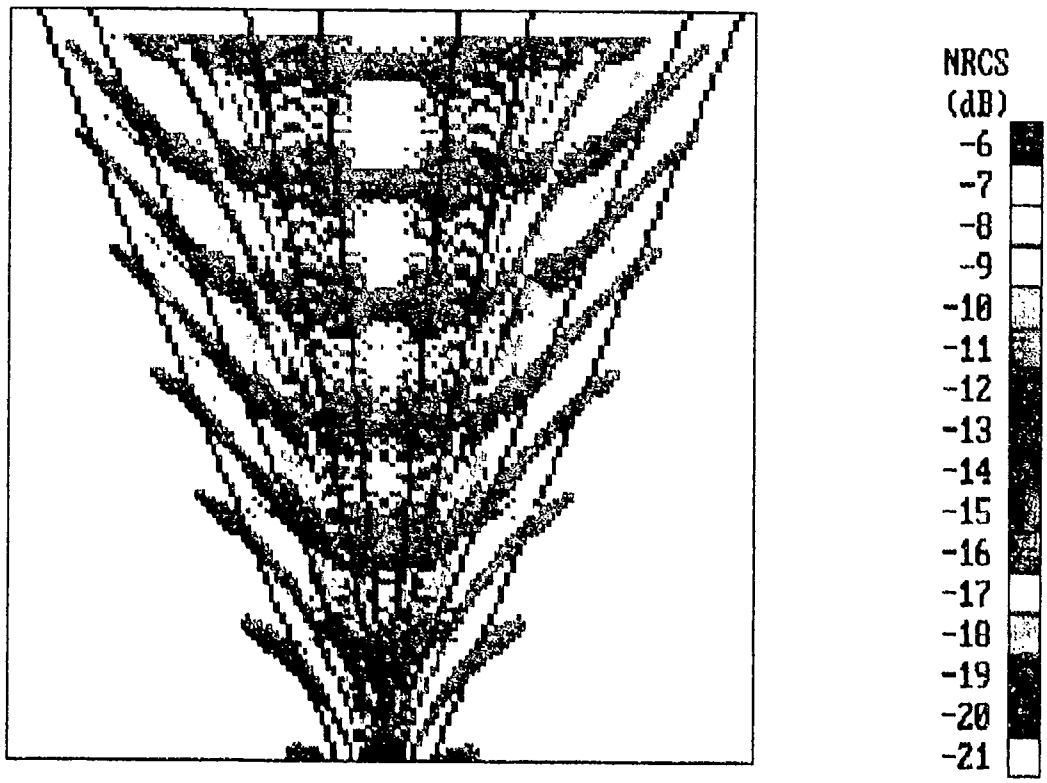

Fig. - 11b The same result as for Fig. 11a, but for vertically polarized incident radiation.

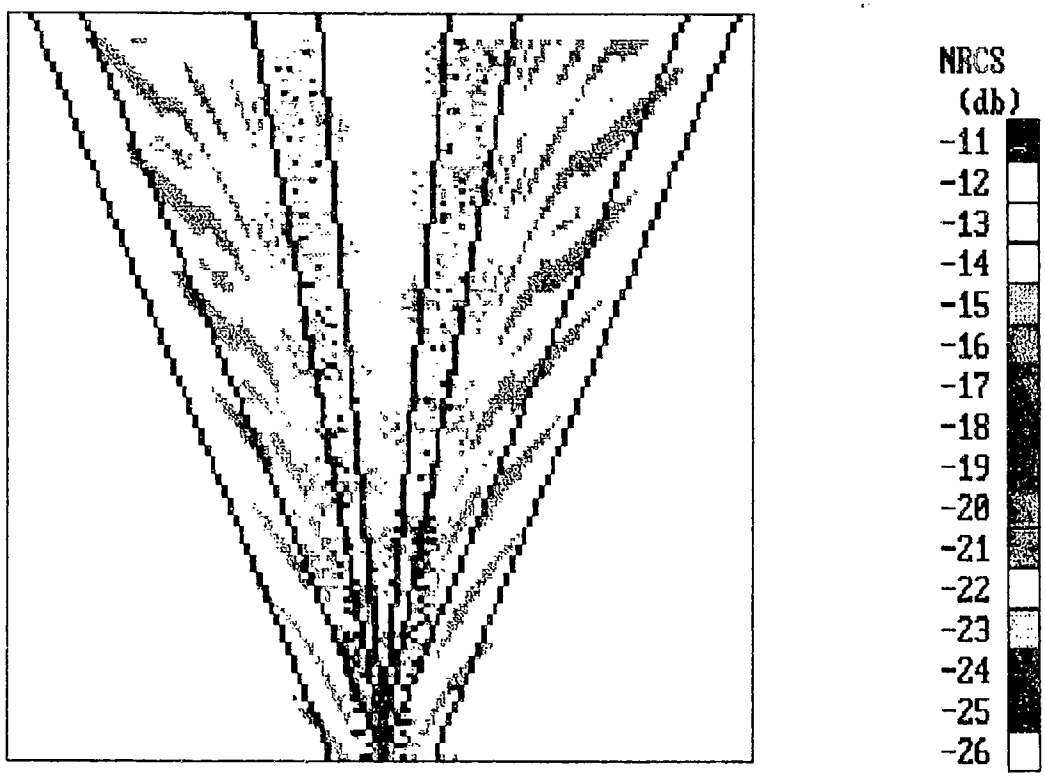

Fig. - 12a The calculated NRCS image for horizontally polarized transmitted radiation, using the wake presented in Figs. 1a-3a, the destroyer at a 25-knot speed, using radar illumination parallel to the axis of the wake.

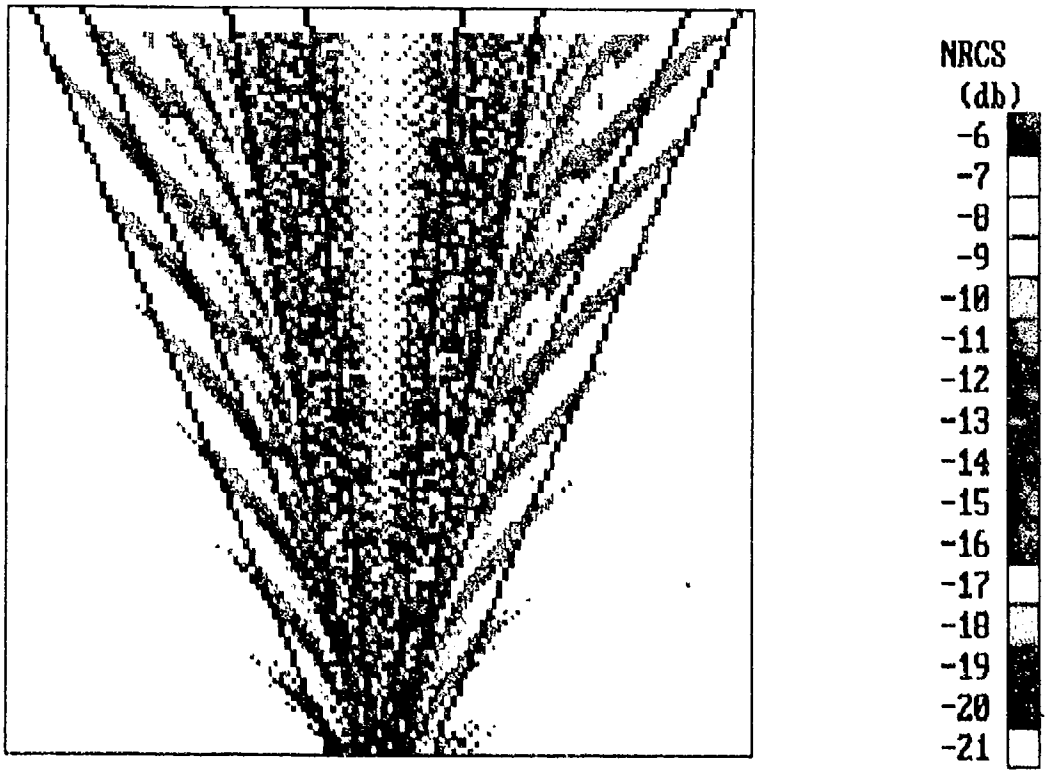

Fig. - 12b The same result as for Fig. 12a, but for vertically polarized incident radiation.

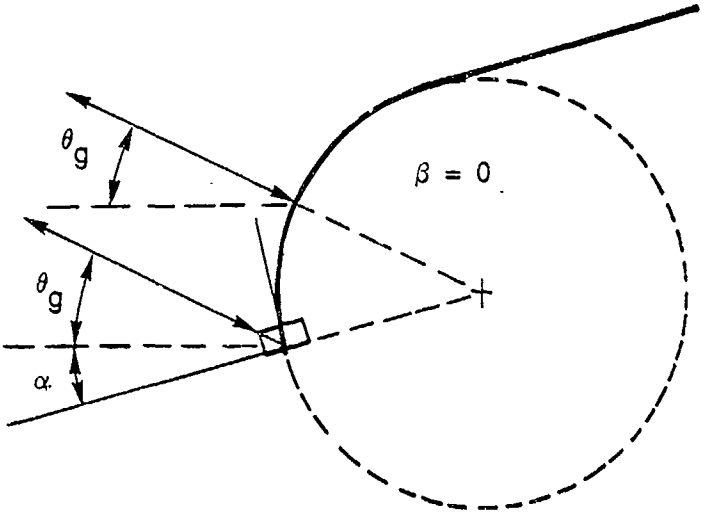

Fig. - 13a A model for a sea spike scatterer suggested by Wetzel, of the form of a half cylinder of water rolling down the face of a long wave. The intersection of the cylinder is perpendicular to the local surface plane.

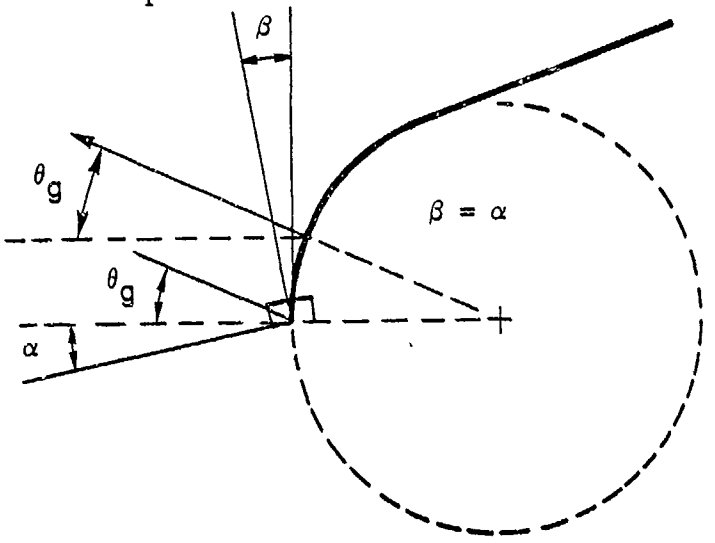

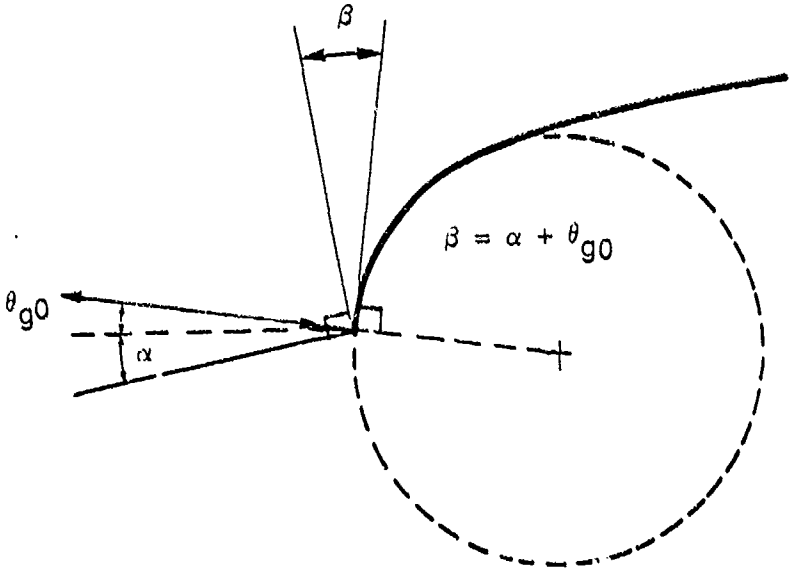

Fig. - 13b,c A model for a sea spike scatterer suggested by Trizna. The first allows scatter for zero grazing angle, while the second is necessary to explain the sudden onset of high RCS observed at 2-deg grazing angle in marine radar experiments.